EXPERIMENTAL AND NUMERICAL INVESTIGATION OF SHOCK-INDUCED FULL VAPORIZATION OF ZINC

R. M. BRANNON and L. C. CHHABILDAS
Sandia National Laboratories, P. O. Box 5800, Albuquerque, NM 87185-0820

Summary—A systematic computational and experimental study is presented on shock-induced full vaporization of zinc resulting from record-high impact speeds recently achieved on the Sandia HyperVelocity Launcher. In these experiments, a thin target plate of zinc is impacted by a tantalum flier plate at speeds ranging from 8 to 10.1 km/s, producing pressures from 3 Mbar to over 5.5 Mbar and temperatures as high as 39000 K (~ 3.4 eV). Such high pressures produce essentially full vaporization of the zinc because the thermodynamic release isentropes pass into the vapor dome near the critical point. To characterize vapor flow, the velocity history produced by stagnation of the zinc expansion products against a witness plate is measured with velocity interferometry. For each experiment, the time-resolved experimental interferometer record is compared with wavecode calculations using an analytical equation of state, called ANEOS, that is known to have performed well at lower impact speeds (less than ~7 km/s) where vaporization is negligible. Significant discrepancies between experiment and calculation are shown to exist under conditions of the more recent higher impact speeds in excess of 7 km/s. Numerical predictions underestimate witness-plate velocity for impact speeds up to about 9 km/s but overestimate witness-plate velocity for impact speeds exceeding 9 km/s. This qualitative change in the character of the discrepancy is conjectured to occur when the temperature on the release isentrope at the critical density lies above the critical temperature. These experiments can be used to develop and refine models representing the dynamics of the shock-induced vaporization process.

INTRODUCTION

Prediction of the interaction between expanded vaporized debris and target materials for applications such as meteorite impact on space vehicles, ballistic penetration of armors, debris shield design, *etc.* demands an accurate treatment of the melting and vaporization process and the kinetics of liquid-vapor propagation. Historically, experimental efforts to understand high-pressure melting and vaporization have been hindered by unavailability of experimental launchers that are capable of speeds needed to induce vaporized states [1]. This problem has been circumvented to some extent by studying materials such as lead, cadmium, and zinc, which have relatively low melting and boiling points [2–4]. For materials of greater programmatic interest (such as aluminum), an alternative is to shock *porous* samples for which irreversible pore collapse enhances heating of the matrix material [5,6]. In this paper, we describe our achievement of record-high impact speeds and resultant vapor concentrations from initially solid zinc. Using the newly-developed HyperVelocity Launcher [7,8], a tantalum flier plate was launched to speeds from 8 km/s to 10.1 km/s, The flier impacted a thin target plate of zinc, producing shock pressures of about 3 Mbar to over 5.5 Mbar, and temperatures as high as 39000 K (~ 3.4 eV). The release isentropes computed from these states pass near zinc's thermodynamic critical point, and it is therefore believed that significant — perhaps *full* — vaporization of the zinc target occurs. To characterize the vapor states, the velocity history produced by stagnation of the expansion products against a witness plate is measured using a velocity interferometer. The amount by which peak witness-plate velocity decreases for increasing distance between the zinc target and witness plate is an indicator of the degree of vaporization. Zinc was chosen for this study because the zinc liquid-vapor co-existence diagram, discussed later, suggests the feasibility of approaching the critical region using our state-of-the-art impact technology. Furthermore, previously-measured experimental data exist for lower-speed impact of zinc [6], and the commonly-used ANEOS equation of state [10] represented these earlier lower-speed lower-pressure experiments for zinc remarkably well.

DISCLAIMER

The purposes of this paper are (1) to report the first experimental results for essentially full vaporization of zinc resulting from shock-compression up to ~5.5 Mbar and ~39000 K and (2) to use these experiments to evaluate the predictions of the ANEOS equation-of-state. The ANEOS equation-of-state is *not* necessarily expected to outperform more modern equations of state. However, because ANEOS is rather well-established (and therefore commonly used), it is important to report any results that limit the model's range of applicability. ANEOS-based calculations have been shown in previous studies [6] to match data for sub-critical shock release of zinc. However, we will show in this paper that for higher shock states, increasing amounts of melting and vaporization of the zinc occur, and one-dimensional ANEOS predictions fail to adequately match the data. The calculations using ANEOS under-predict the interferometer velocity data (and therefore *over*-predict the amount of vaporization) for impact speeds from 8 to 9 km/s, but over-predict the interferometer velocity data (and therefore *under*-predict the amount of vaporization) for impact speeds exceeding 9 km/s. It is conjectured that this reversal of trend occurs once the impact velocity is sufficient to achieve release isentropes that pass above the critical point. The portion of the error attributable to two-dimensional effects (undoubtedly important for vapor propagation distances greater than ~10 mm) is currently under investigation, but the equation-of-state nevertheless seems to contribute to the errors because the *nature* of the errors changes when the zinc release path passes above the critical point. Fundamentally, these results highlight the risk of inaccurate predictions resulting from extrapolating equation-of-state models into pressure/temperature regimes for which they have not been validated.

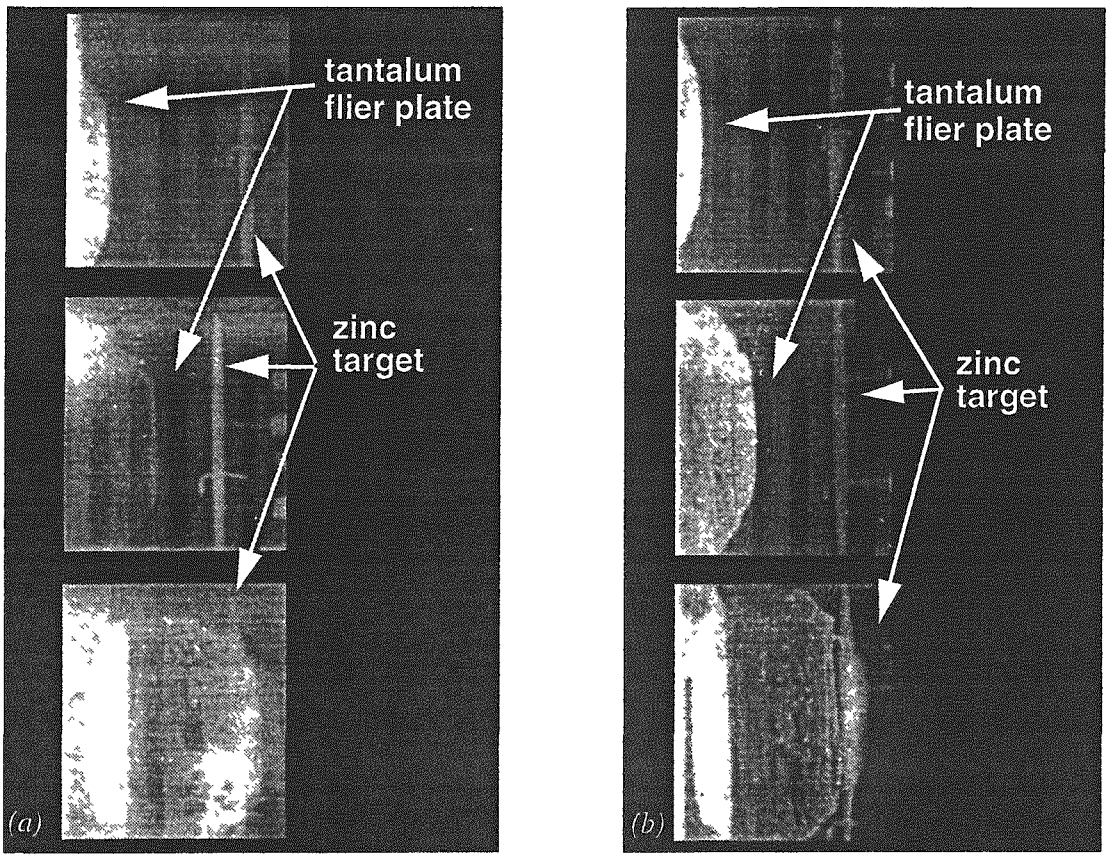

Fig. 1. Tantalum flier plate launched to speeds of *(a)* 8.2 km/s and *(b)* 9.1 km/s. In both experiments, the flier plate traverses 40 mm prior to impacting the thin zinc plate in the final frame.

EXPERIMENTAL TECHNIQUE

The new experiments were performed using the Sandia HyperVelocity Launcher [8,10], which is based on the principle that a structured shockless pressure pulse is required to *ramp* a flier plate up to the desired final velocity to avoid premature melting or fracturing. Flash X-rays were taken to determine the velocity of the flier plate and also to check for its integrity upon acceleration by the shockless pressure-pulse. In Figure 1, radiographs from two representative experiments show that this technique permits the central portion (approximately 19 mm in diameter) of the flier plate to be launched intact and reasonably flat.

The shock vaporization experimental configuration [11] is sketched in Figure 2*(a)*. The target and witness plate were approximately 35 mm in diameter. The lithium-fluoride window was approximately 22 mm in diameter and 25 mm thick in the direction of motion. To minimize effects of flier-plate curvature, the tantalum flier traversed a gap of 40 mm (30 mm for the 10.1 km/s experiments) prior to impacting the zinc target plate.

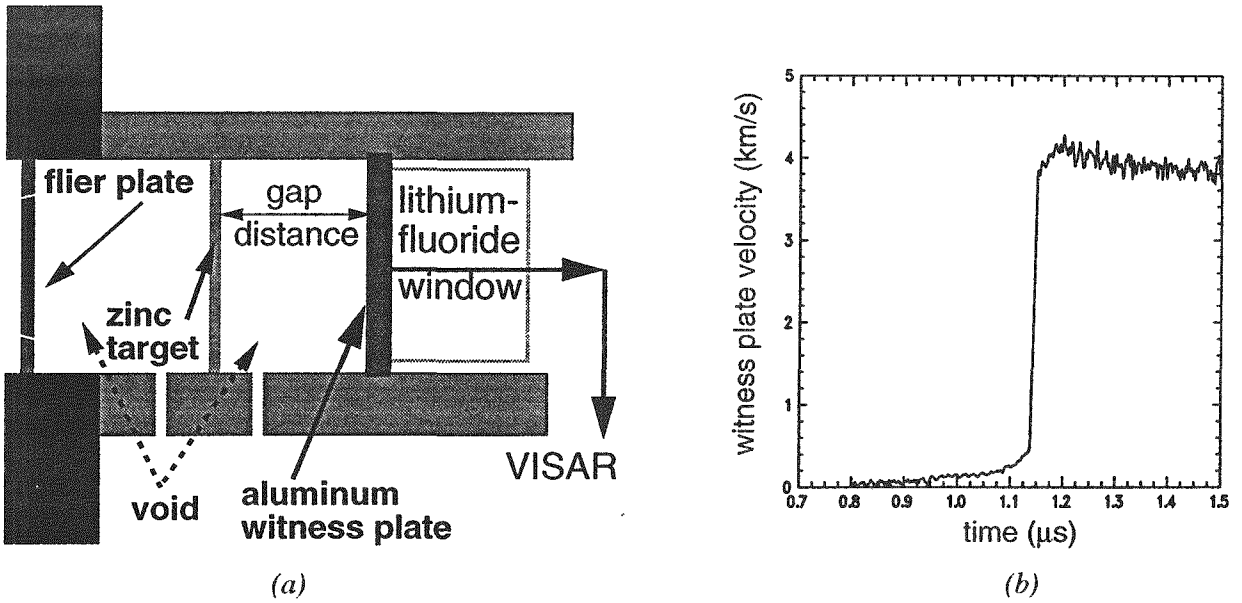

(a) *(b)*

Fig. 2. *(a)* Configuration for vaporization experiments. *(b)* Example VISAR velocity record (for the 8.2km/s, 4 Mbar experiment HZn1) resulting from melted/vaporized zinc stagnating against the aluminum-witness-plate.

Table 1: Impact parameters for shock-induced vaporization experiments

Experiment No.	Tantalum Flier Plate Thickness (mm)	Tantalum Flier Plate Velocity (km/s)	Zinc Target Thickness (mm)	Gap Distance (mm)	Al Witness Plate Thickness (mm)
HZn1[a]	0.215	8.22	0.224	9.99	1.010
HZn2	0.210	9.03	0.229	9.90	1.012
HZn3	0.200	9.1	0.195	9.98	1.970
HZn4	0.210	9.1	0.219	20.09	1.980
HZn6	0.192	10.1	0.179	10.02	1.965
HZn7	0.196	10.1	0.185	9.94	1.996
HZn8	0.201	10.1	0.183	20.05	1.996
HZn9	0.197	10.1	0.179	5.04	2.000
HZn10	0.198	10.1	0.177	19.99	2.004
HZn11	0.213	10.1	0.179	5.01	1.999
HZn12	0.216	10.1	0.174	0.00	1.969
ZnVAP1[b]	2.049	5.891	1.836	4.841	1.907
ZnVAP2[b]	2.039	5.948	1.817	10.002	1.925
ZnVAP3[b]	0.499	6.822	0.893	5.012	1.937
ZnVAP4[b]	0.505	6.874	0.902	10.022	1.907

a. Note that the main HZn parameters being varied are gap size and flier impact speed.
b. The ZnVAP experiments were conducted by Wise et al. [6] with a two-stage light-gas gun.

(The flier-plate velocity was not measured in every experiment because electrical noise generated during pulsed X-ray discharge affected the velocity interferometer signal; a few velocity calibration tests were therefore performed to estimate the flier-plate impact velocity to within two percent.) Impact of the flier

against the zinc plate produced a debris cloud of rarefied liquid-vapor zinc which was permitted to traverse a gap of known dimensions before stagnating against an aluminum witness plate. The subsequent particle velocity history (*e.g.*, Fig 2*(b)*) at the witness-plate/window interface was measured using a velocity interferometer [12], commonly referred to as VISAR. Multiple experiments were performed using different fringe sensitivities to determine unique particle velocities. In experiment HZn11 (Table 1), an interferometer having a dual delay leg was used to measure the peak particle velocity resulting from the stagnation pressure history of the vaporized products. An aluminum witness-plate thickness of 2 mm was found to be most effective in obtaining particle-velocity history measurements because thinner witness-plate dimensions of 0.5 mm and 1.0 mm resulted in a premature loss of laser light intensity and fringe information. Table 1 lists relevant impact parameters for our experiments as well as for a series of earlier similar experiments [6].

NUMERICAL MODEL DESCRIPTION

The Sandia wave propagation code CTH [13] was used to simulate the experiments. The thermomechanical response of the materials was modeled using the ANEOS analytical equation-of-state package [9,14], which handles solid, liquid, vapor and mixed phases in a complete thermodynamically consistent semi-empirical manner and is well established in CTH. ANEOS was selected because it is known to agree well with experimental data for zinc at lower impact speeds [6]. The ANEOS input parameters employed in our simulations (Table 2) are identical to those used in [6].

Table 2: Material properties used in ANEOS equation of state *(units are cgs– eV)*

ANEOS Parameter	No.	Zinc	Aluminum	Tantalum	LiF
Reference density	V3	7.14	2.7	16.654	2.601
Reference temperature	V4	0.02567785	0.02567785	0.02567785	0.02567785
Reference pressure	V5	0.	0.	0.	0.
Sound speed / bulk modulus if positive	V6	-3.e5	7.63e11	-3.414e5	-5.148e5
Reference Gruneisen coefficient	V7	1.6	2.06	1.6	1.668
Debye temp, complete functions if <0	V8	0.0278	0.0343	-0.0218	-0.0665
Slope of linear U_s-u_p / switch if <0	V9	1.3	-1.5	1.201	1.353
3*Gruneisen coefficient	V10	2	2	2	2
Zero temp separation energy	V11	2.9E10	1.2E11	4.322E10	3.9083E11
Melting temp, melt energy if <0	V12	0.0589	-6.639E9	0.2817	0.1021
C53 parameter for low-density P_c	V13	6.986E11	3.5E12	0	0
C54 parameter for low-density P_c	V14	0.8594	0.8	0	0
H_o in *conductivity*=$H_o(T)^{C41}$	V15	0	2.7E11	0	0
C41 in *conductivity*=$H_o(T)^{C41}$	V16	0	0	0	0
Lowest allowed solid density	V17	5.89826	2.305	0	0
Heat of fusion for melt transition	V23	1.12E9	3.98E9	1.746E9	0
Ratio of liquid to solid density at melt	V24	0.96	0.938	0.957	0

Several release isentropes for zinc (generated using the ANEOS parameters listed above) are shown in Figure 3. The isentropes for the current (HZn) experiments are those that pass close to the critical point. The zinc critical point data predicted by ANEOS are: density=2.751 g/cm^3, temperature = 0.2736 eV = 3175 K, and pressure = 4.085 kbar. As mentioned earlier, zinc was selected for the current work in part because of its low melting/vaporization points as shown by the phase curve in Figure 3. This advantage of zinc is further highlighted by comparing the zinc phase diagram (Fig. 3) with similar plots for tantalum and aluminum (Fig. 4), which we have plotted at the same pressures to emphasize the qualitative phase differences that make zinc the more attractive material for studying shock-induced vaporization (a more fair comparison would be to plot isentropes corresponding to the entropies achievable for the same tantalum flier-plate speeds).

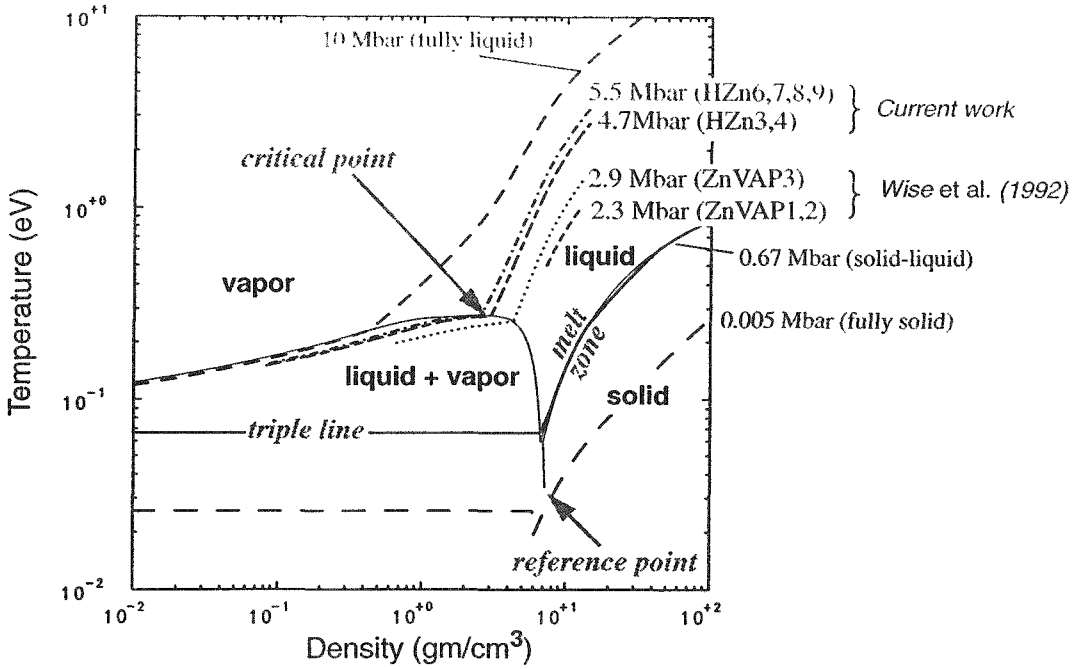

Fig. 3. Zinc release isentropes plotted over the range of densities and pressures numerically predicted for the experiments. For each curve, the constant value of entropy is the zinc Hugoniot entropy associated with the labeled Hugoniot pressure. Isentropes labeled 0.005 Mbar, 0.67Mbar, and 10 Mbar represent release from fully-solid, solid-liquid, and fully-liquid Hugoniot states respectively, and are provided for reference (i.e., they do not correspond to actual experiments).

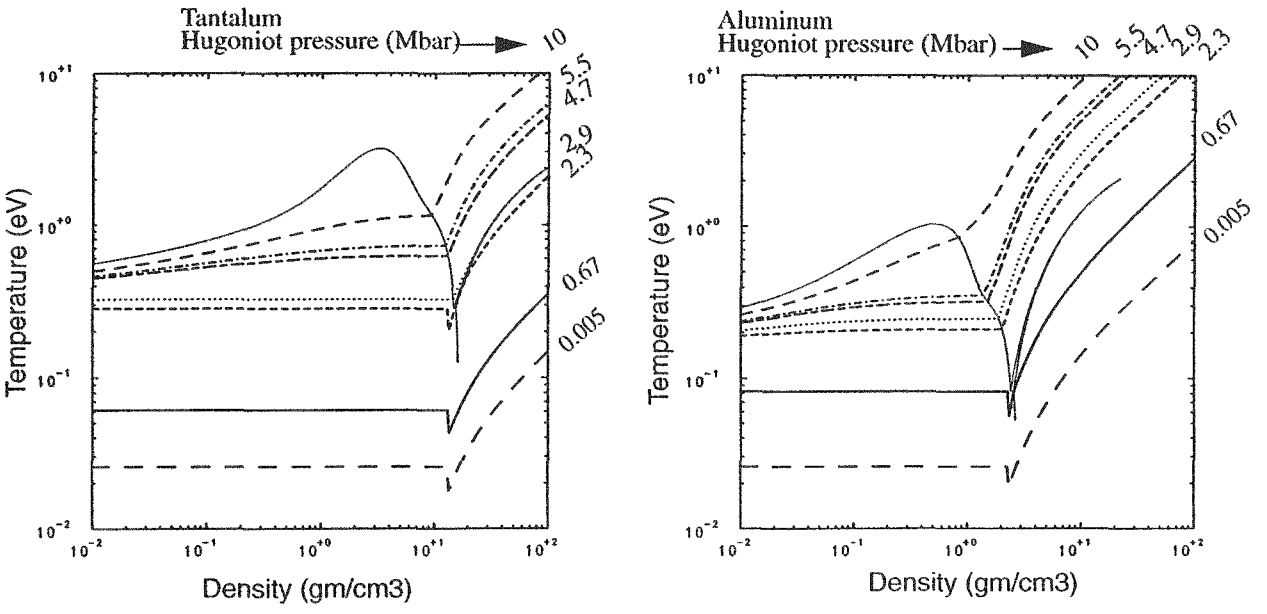

Fig. 4. Release isentropes for (a) tantalum and (b) aluminum. The lines of constant entropy correspond to the Hugoniot entropy at the labeled Hugoniot pressures, which have been selected to be the same as those in Fig. 3 for ease of comparison.

EXPERIMENTAL AND COMPUTATIONAL RESULTS

This section reports the results from the eleven experiments designated HZn in Table 1 that were performed for flier-plate impact velocities from 8.2 km/s to 10.1 km/s. Also reported in this section are the computational simulations of the experiments. Detailed analysis and interpretation of the results will be deferred until the discussion section. There is no time fiducial: the time scales of the experimental records are adjusted to overlap the calculated records at the mid-range point on the initial rise curve. For all calculations, "time zero" is when the tantalum flier plate impacts the zinc target.

Results of Experiments at 8.22 km/s (~ 4 Mbar Impact Stress).

Experiment HZn1 was conducted at an impact velocity of 8.22 km/s. At this velocity, zinc is shocked to a computed level of ~ 4 Mbar. The liquid-vapor state induced upon release is allowed to traverse a gap of ~ 10 mm until it stagnates against an aluminum witness plate. The particle velocity history measured at the witness-plate/LiF-window interface (see Fig. 2*(a)*) is compared with the ANEOS/CTH numerical prediction in Figure 5. The measured peak velocity is ~ 4.2 km/s. Only one experiment was conducted at this impact stress. Speculations about the extremely poor numerical results are in the discussion section. Of course, consistency calculations against prior experiments were performed to check the ANEOS data (see Figure 10).

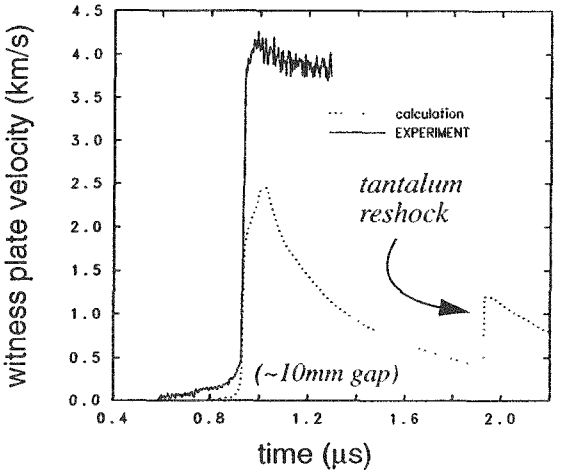

Fig. 5. Experiment result for the 8.22 km/s shot HZn1 compares unfavorably with the ANEOS calculation.

Results of Experiments at 9.1 km/s (~ 4.7 Mbar Impact Stress).

Experiments HZn2, HZn3, and HZn4 are each for an impact velocity of 9.1 km/s. Upon impact, a computed stress of ~ 4.7 Mbar is introduced in the zinc sample. Material in the subsequent *released* liquid-vapor states propagates across a gap of up to 20 mm, before stagnating against an aluminum witness plate. The measured and computed particle velocity histories are shown in Figure 6. Experiments HZn2 (not shown) and HZn3 were very nearly the same except that HZn3 utilized a witness plate two times thicker than that used in experiment HZn2. The lower particle velocity measured in experiment HZn3 is a result of the thicker aluminum witness plate which led to wave attenuation effects when compared to experiment HZn2. Vaporization is evident because as the propagation distance (*i.e.*, gap size) increases, the peak amplitude decreases while the rise time of the wave increases. For *this series* of experiments, calculations under-predict velocity, implying that they *overestimate* the amount of vaporization. Counterintuitively, as discussed in the next section, the numerical prediction improves at *late* time (i.e., for larger gap size). Recall that the *lower-speed* experiment HZn1 (Fig 5) uses a witness-plate that is roughly half the thickness of that used in the 9.1 km/s experiment HZn3 (Fig 6*(a)*); so attenuation across the buffer explains why the two numerical calculations show roughly the same peak velocity at the witness-plate/window interface. In contrast, the experimental records for HZn1 and HZn3 show a pronounced *decrease* in peak velocity as flier impact speed is increased, which is evidence of increased amounts of vaporization at higher impact speeds. These important features of the experiments and computations will be explored further in the discussion section.

Results of Experiments at 10.1 km/s (~ 5.5 Mbar Impact Stress).

Experiments HZn6 through HZn12 are each for an impact velocity of 10.1 km/s. Upon impact, a computed stress state of over 5.5 Mbar is introduced in the zinc sample. The measured and computed particle velocity histories for experiments HZn7, HZn8 and HZn9 are shown and compared to predictions in Figure 7. These experiments are discussed further in the next section.

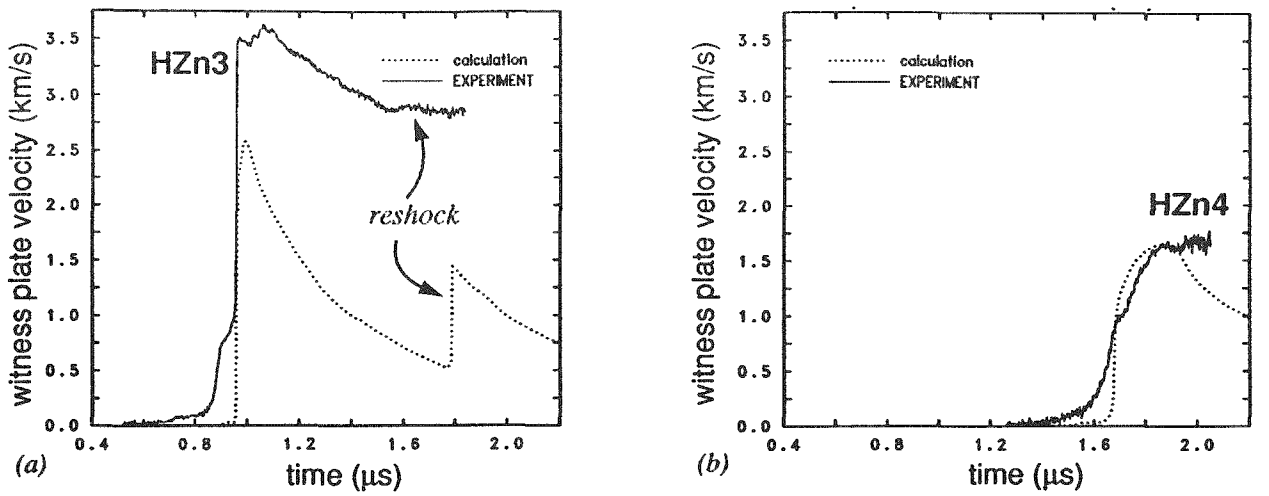

Fig. 6. Measured and calculated VISAR particle velocities for experiments conducted at approximately 9.1 km/s for a gap size of *(a)* ~10 mm and *(b)* ~20 mm. The reshock (not pronounced in the experiments) results from recompression by the tantalum.

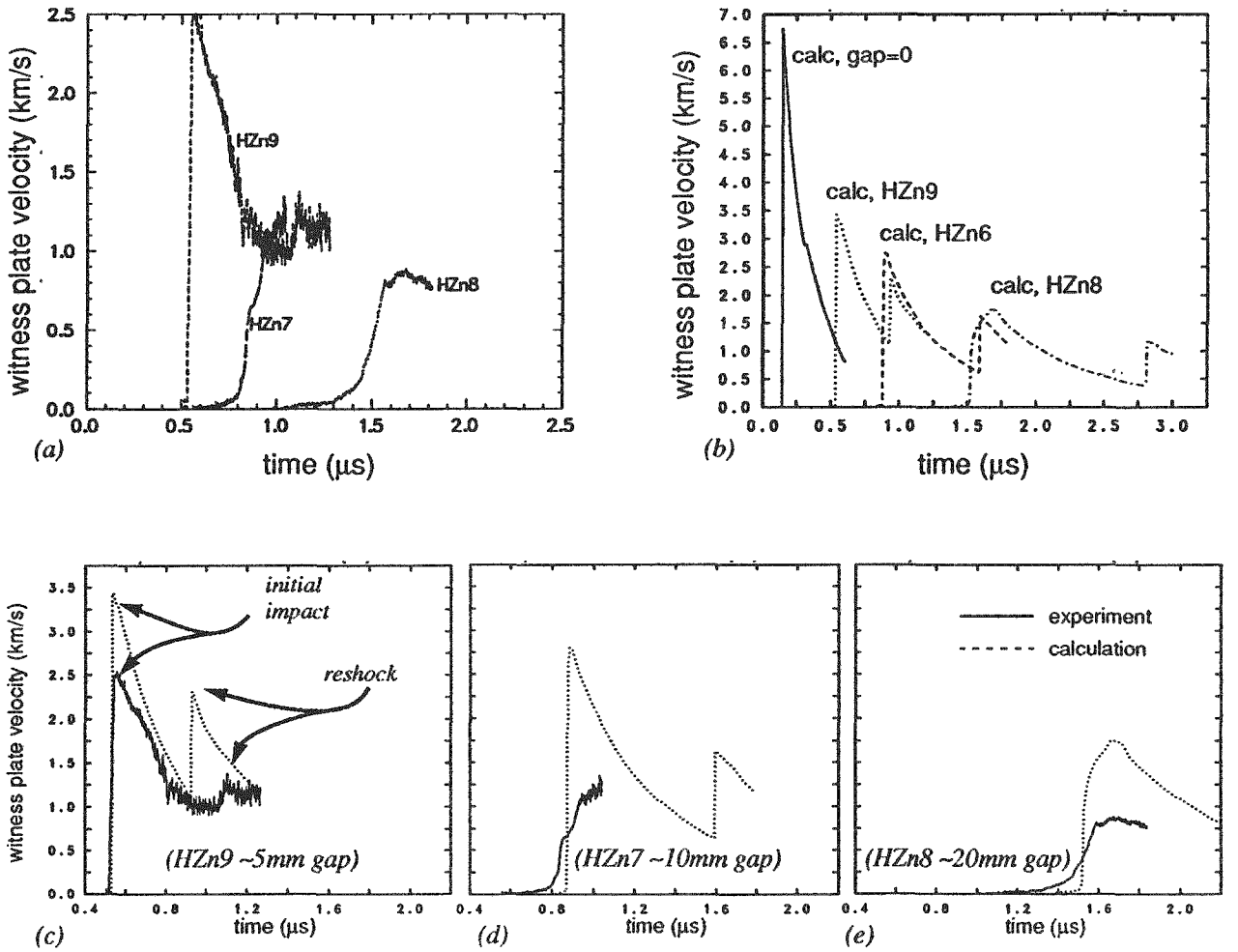

Fig. 7. *(a)* Measured and *(b)* calculated particle velocity histories for experiments conducted at approximately 10.1 km/s; *(c)*, *(d)*, and *(e)* show individual comparisons between calculations and experiments for varying gap size (as labeled) with the time scales aligned at mid-range.

Specific Volume.

Figure 8 shows a plot of numerically predicted specific volume *vs.* time for seven Lagrangian points distributed evenly throughout the zinc target material for the 10.1 km/s calculations. The strong tendency toward a linear increase in volume with respect to time is consistent with free expansion of a vapor. Note also that most of the vaporization occurs near the *impact side* of the target. Somewhat smaller amounts of vaporization occur at the free surface. The region of least expansion lies in the target interior about one fourth of the plate thickness from the free surface.

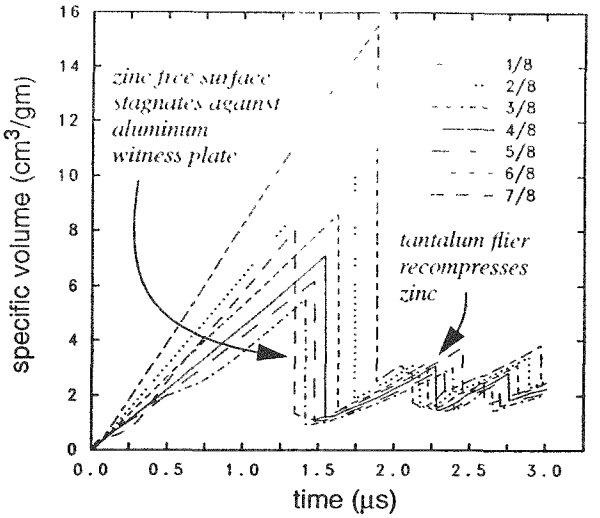

Fig. 8. Specific volume vs. time for several Lagrangian points in the zinc target. A legend label n/8 refers to a point that is n/8ths of the zinc target plate thickness away from the impact side.

Dependence of Peak Particle Velocity Measurements on Propagation Distance.

In both sets of experiments conducted at 9.1 km/s and 10.1 km/s, the measured peak particle velocity produced by the liquid-vapor states stagnating at the aluminum witness plate depends on the propagation distance (i.e., on gap size). The change in peak witness-plate velocity with respect to gap size is a strong indication of the amount of vaporization that occurs in the zinc over time. Table 3 lists the peak witness-plate velocity measured for each experiment. This table also lists values for the peak velocity normalized with respect to the tantalum impact velocity V and zero-gap velocity U_{max}, respectively, where U_{max} is the peak witness-plate velocity for a gap size of zero. The value of U_{max} is based on calculations. The variation of measured peak witness-plate velocity with respect to gap size (evident in Table 3) is shown graphically in Figure 9.

Table 3: Results of shock-induced vaporization experiments

Experiment Name	Gap distance (mm)	Impact velocity, V (km/s)	Peak witness plate velocity, u_{wp} (km/s)	Zero-gap witness plate velocity[a], U_{max} (km/s)	$\frac{u_{wp}}{V}$	$\frac{u_{wp}}{U_{max}}$
HZn1	9.99	8.22	4.14	6.3	0.504	0.657
HZn2	9.90	9.03	3.81	6.55	0.422	0.591
HZn3	9.98	9.1	3.61	6.45	0.397	0.560
HZn4	20.09	9.1	1.67	6.45	0.184	0.256
HZn12	0	10.1	---[b]	6.85	---[b]	---[b]
HZn9	5.04	10.1	2.50	6.85	0.248	0.365
HZn11	5.01	10.1	2.32	6.85	0.230	0.339
HZn7	9.94	10.1	1.22	6.85	0.121	0.178
HZn6	10.02	10.1	0.50	6.85	0.050	0.073
HZn8	20.05	10.1	0.90	6.85	0.089	0.131
HZn10	19.99	10.1	0.34	6.85	0.034	0.050
ZnVAP1[c]	4.841	5.891	4.7	4.72	0.798	0.996
ZnVAP2[c]	10.002	5.948	4.7	4.72	0.790	0.996
ZnVAP3[c]	5.012	6.822	4.7	5.4	0.689	0.870
ZnVAP4[c]	10.022	6.874	4.25	5.4	0.618	0.787

a. Computed values.

b. Experiment HZn12 (zero gap) failed by loss of contrast in the velocity interferometer signal, suggesting loss of window transparency.

c. Earlier experiments [6] employed different plate thicknesses — see Table 1.

Computational Predictions of Peak State.

Table 4 shows the ANEOS/CTH numerical predictions of the Hugoniot peak density, pressure, and temperature reached in the target immediately following impact of the tantalum flier. It is from these peak states that the zinc expands upon release, following a path along an isentrope illustrated in Figure 3. The peak values listed in the table are for the initial shock state only; once the expansion products stagnate against the witness plate, temperature increases to values higher than listed in Table 4. The peak free-surface velocities listed in Table 4 are achieved not during the primary shock compression, but are approached asymptotically in time as the liquid/vapor products expand (this asymptotic value was read from Lagrangian particle-velocity plots for all calculations).

Table 4: Calculation predictions of peak states in the zinc target during gap crossing

Experiment name	**Impact Velocity** (km/s)	**peak density** (g/cm^3)	**peak pressure** (Mbar)	**peak temperature** (K)	**peak free-surf. velocity** (km/s)
ZnVAP1,2[a]	5.9	12.5	2.3	12000	9.5
ZnVAP3[a]	6.8	13.0	2.9	17000	10.5
HZn1	8.22	13.7	4.0	25000	11.9
HZn3,4	9.1	14.2	4.7	31000	13.5
HZn6,7,8,9	10.1	14.5	5.5	39000	15.5

a. The peak values listed for the previous studies [6] were obtained by *our own* duplications of those calculations (see, for example, Figure 10).

DISCUSSION

Previous studies. Similar investigations [6] were previously performed at impact velocities of ~ 5.9 km/s and 6.8 km/s, where the zinc sample was shocked to ~ 2.3 Mbar and 2.9 Mbar, and the release products were allowed to traverse a gap of 10 mm before stagnating against an aluminum witness plate backed by a lithium-fluoride window. Shocks were observed at the interferometer window, suggesting that very little vapor had been produced. For the impact experiments performed at ~ 5.9 km/s, the measured peak particle velocity did not vary with propagation distance (see Figure 9), suggesting that the zinc target plate did not vaporize. For the impact velocity of ~ 6.8 km/s, the peak particle velocity dropped off with gap size (suggesting vaporization), but shocks continued to be observed at the witness-plate/laser-interferometer window interface. Presumably, a small-amplitude ramped loading at the interface had been overdriven by the subsequent large-amplitude shock.

Rise times. For our study, having the impact velocity increased to 8.22 km/s, 9.1 km/s, and 10.1 km/s, finite rise times were observed in the interferometer velocity records. The measured rise time increases with increasing propagation distance for the same impact velocity (see, *e.g.*, Figs. 7*(c)*, 7*(d)*, and 7*(e)*) and with increasing impact velocity for the same propagation distance (see, *e.g.*, Figs. 5, 6*(a)*, and 7*(d)*).

Density distributions for several impact velocities have been measured *for lead* using X-ray techniques [3], and it has been speculated [3,15] that the leading edge of the debris cloud consists of fast-moving low-density vapor products followed by slower-moving higher-density products, leading to a time-dependent loading on the aluminum witness plate and consequent finite rise-time measurements. It is not surprising that the rise time increases with increasing propagation distance because the size of the liquid-vapor cloud (column) will increase linearly with time provided there are negligible time-dependent effects associated with the vaporization process itself. If the vaporization process is time-dependent — *i.e.*, if more material vaporizes at late time due to super-heating effects — then there should even be more vapor present with increased time (or, equivalently, with increased propagation distance). In other words, physically realistic vaporization doesn't occur instantaneously. To properly model these experiments, explicit treatment of boiling kinetics may be necessary.

Interferometer particle velocity measurements. The aluminum witness-plate/lithium-fluoride window can be regarded as a target with which the liquid/vapor debris cloud interacts. The peak interface velocity measurement u_{wp} is an indicator of the maximum stress resulting from this interaction. Observe that the measured peak velocities are *higher* for the *lower*-speed 9.1 km/s shots (Fig. 6) than for the corresponding 10.1 km/s shots (Fig. 7), which suggests that greater vaporization occurred in the 10.1 km/s

shots. Figure 9 (which summarizes experimental data in Table 3 and Figures 5, 6, and 7) shows that the peak witness-plate velocity u_{wp} and, therefore, the target/debris interaction stress decrease monotonically with increasing propagation distance (gap size). All curves in Figure 9 must — in one-dimensional theory – asymptote to some constant value as gap size is increased. When such a curve asymptotes to *zero*, the sample must have vaporized completely. When a curve asymptotes to some non-zero value of u_{wp}/U_{max}, the sample must have only partially vaporized. When a curve is *constant*, no vaporization must have occurred and the maximum interaction stress must be independent of gap size. In Figure 9, the lowest speed experiment (5.92 km/s) exhibits negligible expansion (*i.e.*, the zinc target remains essentially intact as it crosses the gap). By contrast, the highest speed (10.1 km/s) experiment shows considerable expansion of the zinc, which corresponds to a much lower stress on the buffer than the lower-speed lower-vaporization experiments. (Even though loading stress can be reduced substantially by vaporization, the survivability of any target nevertheless depends on many other parameters including, the duration of the pressure pulse, the thickness of the target, and the yield and fracture strength of the target.) For zinc, the rapid approach to an asymptotic limit suggests that boiling occurs more rapidly from super-critical states.

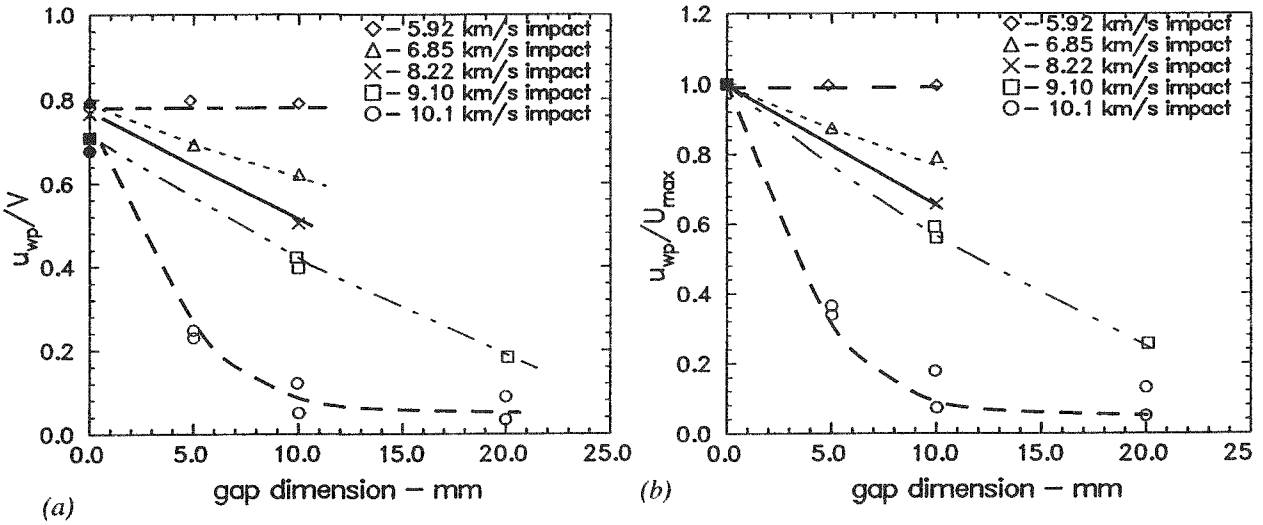

Fig. 9. Normalized measured witness-plate peak velocity vs. propagation distance (i.e., gap size). The normalization factors are *(a)* tantalum impact velocity V and *(b)* the computed zero-gap peak velocity U_{max} (which depends on tantalum impact speed and experiment geometry).

Comparison with calculations. The quality of agreement between calculations and experiments depends on the stress regime from which the zinc is allowed to expand. Previous studies [6] indicate that the current ANEOS model is quite adequate for lower impact speed events where the material does not vaporize. *These previous calculations were duplicated (see Fig. 10) to ensure validity of the ANEOS parameters listed in Table 2.* At the higher impact speeds used in our study, there is a substantial discrepancy between experiments and calculations. Unlike previous studies of lead [3], the ANEOS numerical predictions underestimate the witness-plate velocity (overestimate vaporization) for the sub-critical (see Figure 3) experiments HZn1-4 and overestimate the witness-plate velocity (underestimate vaporization) for the super-critical experiments HZn6-9.

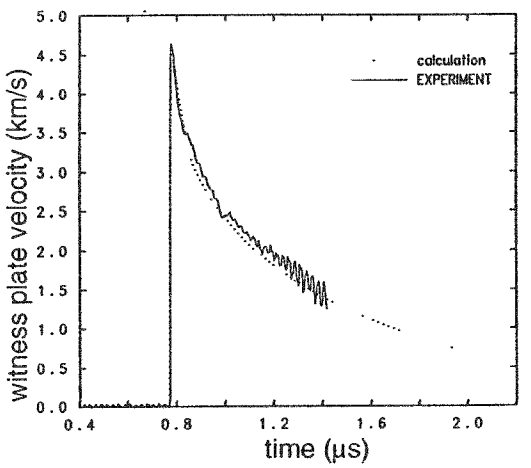

Fig. 10. Duplication of the Wise *et al.* lower-speed lower-pressure ANEOS calculation [6], performed to ensure that the material data used to model the new experiments continued to yield good agreement with the older experiments.

Numerical predictions of interferometer velocity for the 10.1 km/s shots increasingly disagree with data as gap size is increased whereas similar predictions for 9.1 km/s shots *improve* as gap size is increased. However, the quantity $(1\text{-}u_{wp}/U_{max})$ may serve as a measure of the degree of vaporization. Thus, one measure of the error in calculated vaporization (to be applied when vaporization is significant) is

$$E_{vap} = \frac{u_{wp} - u_{wpCALC}}{U_{max} - u_{wp}} \quad (1)$$

where u_{wp} is the experimentally measured value of the peak witness plate interferometer velocity, and u_{wpCALC} is the numerically predicted value of u_{wp}. The 10.1 km/s calculations have vaporization errors of approximately -41%, -27%, and -15% for gap sizes of ~5mm, ~10mm, and ~20mm, respectively. Negative errors indicate that these calculations underpredict the amount of vaporization. The 9.1 km/s calculations have vaporization errors of approximately 37% for a gap of ~10 mm and nearly 0% for a gap of ~20 mm. Note that for both impact speeds, *the magnitudes of the vaporization errors decrease with increasing gap size*. This result suggests that perhaps there is a vaporization delay (such as a superheating at very early times) occurring in the experiments that is not captured by the ANEOS model which assumes instantaneous response. The lower vaporization errors seen in the 10 km/s experiments may indicate that boiling kinetics may not play so strong a role above the vapor dome.

CONCLUSIONS

In this work, a systematic computational and experimental study was performed to enhance understanding of shock-induced vaporization of zinc. Using record-high impact velocities achieved with the Sandia HyperVelocity Launcher, zinc was shocked to thermomechanical states sufficiently energetic to produce significant vaporization upon release. The velocity history produced by stagnation of the expansion products against a witness plate was measured at an aluminum/lithium-fluoride window interface using a velocity interferometer. The measured experimental data for zinc were compared with wavecode calculations using an analytical equation of state, referred to as ANEOS. Some of the key results of the present experiments and simulations are:

- Zinc was shocked over the calculated stress range of 3 Mbar to over 5.5 Mbar, and calculated temperatures over the range of 25000 K to 39000 K. In the present investigation, the release products were allowed to propagate over a distance of up to 20 mm (~100 times the zinc plate thickness).
- Finite rise times are observed at an aluminum/lithium-fluoride window interface, suggesting that there is a density-velocity distribution in the expanded debris cloud.
- The measured rise time (resulting from the stagnating debris products) increases with increasing propagation distance holding impact velocity constant, as well as with increasing impact velocity holding propagation distance (gap size) constant.
- Measured peak witness-plate velocity decreases with increased propagation distance (see Fig. 9), suggesting at least partial zinc vaporization. The peak witness-plate velocity decreases with increasing impact velocity (holding propagation distance constant).
- Both the rise time and peak velocity measurements suggest an increased vapor concentration in the expanded debris products when zinc is shocked and released from stress states above 2.9 Mbar. There is no evidence of vaporization over propagation distances of 10 mm when zinc is shocked and released from a stress state of 2.3 Mbar.
- Release isentropes calculated using the ANEOS equation of state for zinc suggest that the release isentrope from 5.5 Mbar passes above the critical point.
- There is a discrepancy between experimental measurements and numerically predicted witness plate velocities when zinc is shocked by tantalum at speeds in excess of 7 km/s. Interestingly, the calculated plate velocities are underestimated for impact speeds up to 9 km/s, and overestimated at speeds of 10 km/s. At impact speeds over the velocity regime of 7 to 9 km/s, the calculations seem to predict a higher concentration of vapor than experiments, whereas at an impact speed of 10 km/s, the calculations predict a lower concentration of vapor.
- Part of the discrepancy between experimental results and ANEOS predictions may be related to a time-dependent vaporization process which is not modeled in the calculations.

Ours are the first time-resolved measurements of shock-induced vaporization where the release isentrope is believed to pass above the critical point. Natural extensions of this work include: (1) further quantify these measurements with estimates of vapor fractions in the expanded debris products; (2) perform two-dimensional calculations (this may be prohibitively costly due to the extremely refined mesh required), (3) adjust the ANEOS critical point parameters to better match experiments (if possible), (4) explore more sophisticated alternatives to ANEOS to better match the data, (5) enhance the ANEOS model itself to include theoretical critical point models such as those discussed in [16] or to include boiling kinetics, (6) modify the experiment design to shock porous and/or high-temperature zinc at higher impact velocities in order to release zinc from substantially higher temperatures and into vapor states directly.

ACKNOWLEDGMENTS

This work performed at Sandia National Laboratories supported by the U.S. Department of Energy under contract number DE-AC04-94AL85000. W. D. Reinhart and C. A. Hall are acknowledged for their support in conducting experiments. Assistance from Tim Trucano and Marlin Kipp in performing calculations is gratefully acknowledged.

REFERENCES

1. A. V. BUSHMAN and V. E. FORTOV, Wide-range equations of state for matter under extreme conditions. *Sov. Tech. Rev. B. Therm. Phys.* **2**, 219–336 (1987).
2. J. R. ASAY, T. G. TRUCANO, and L. C. CHHABILDAS, Time-resolved measurements of shock-induced vapor-pressure profiles. In: *Shock Waves in Condensed Matter - 1987* (Eds., S. C. Schmidt and N. C. Holmes), pp. 159-162, Elsevier Science Publishers B. V. (1988)
3. J. R. ASAY and T. G. TRUCANO, Studies of density distributions in one-dimensional shock-induced debris clouds. *Int. J. Impact Engng.* **10**, 35-50. (1990).
4. S. A. MULLIN, C. E. ANDERSON, JR., and J. S. WILBECK, Dissimilar material scaling relationships for hypervelocity impact. Prepared by Southwest Research Institute for Defense Nuclear Agency under contract DNA001-86-C-0037, Project 06-1039-001, DNA-TR-89-112, July 1990. (1990).
5. G. I. KERLEY, and J. L. WISE, Shock-induced vaporization of porous aluminum. In: *Shock Waves in Condensed Matter - 1987* (Eds., S. C. Schmidt and N. C. Holmes), pp. 155-158, Elsevier Science Publishers B. V. (1988).
6. J. L. WISE, G. I. KERLEY, and T. G. TRUCANO Shock-vaporization studies on zinc and porous carbon. In: *Shock Compression of Condensed Matter 1991*, (Eds., S. C. Schmidt, R. D. Dick, J. W. Forbes, D. G. Tasker), pp. 61-64, Elsevier Science Publishers B.V. (1992).
7. L.C. CHHABILDAS, L.M. BARKER, J.R. ASAY, T.G. TRUCANO, G.I. KERLEY and J.E. DUNN, In: *Shock Waves in Condensed Matter - 1991* (Eds., S. C. Schmidt, R. D. Dick, J. W. Forbes, and D. G. Tasker), p. 1025, Elsevier Science Publishers B. V. (1992).
8. L. C. CHHABILDAS, L. N. KMETYK, W. D. REINHART, and C. A. HALL, Enhanced hypervelocity launcher - capabilities to over 16 km/s. This volume. (1994).
9. S.L. THOMPSON and H.S. LAUSON, Improvements in the CHARTD Radiation-Hydrodynamics Code III: Revised Analytic Equation of State, *Report SC-RR-710714*, Sandia Laboratories, Albuquerque, New Mexico (1972).
10. L. C. CHHABILDAS, J. E. DUNN, W. D. REINHART, and J. M. MILLER, An impact technique to accelerate flier-plate velocities to over 12 km/s. *Int. J. Impact Engng.* **14**, 121-132 (1993).
11. J. L. WISE and L. C. CHHABILDAS, Laser interferometer measurements of refractive index in shock compressed materials. In: *Shock Waves in Condensed Matter* (Ed., Y. M. Gupta), pp. 441-454, Plenum Press, N.Y. (1986).
12. L. M. BARKER and R. E. HOLLENBACH, Laser interferometer for measuring high velocities of any reflecting surface. *J. Appl. Phys.* **43**, pp. 4669-4675. (1972).
13. J.M. MCGLAUN, S.L. THOMSON, and M.G. ELRICK, CTH: A three-dimensional shock-wave physics code, *Int. J. Impact Engng.* **10**, 351-360 (1990).
14. S.L. THOMPSON, ANEOS Analytic Equations of State for Shock Physics Codes Input Manual. Sandia National Laboratories report SAND89-2951, working draft May 1990. (1990).
15. L. C. CHHABILDAS, E. S. HERTEL, and S. A. HILL, Hypervelocity impact tests and simulations of single whipple bumper shield concepts at 10 km/s. *Int. J. Impact Engng.* **14**, 133-144. (1993).
16. M.A. ANISIMOV AND S.B. KISELEV, Thermophysical properties of liquids and liquid solutions in the critical region. *Sov. Tech. Rev. B. Therm. Phys.* **1**, 337-424 (1987).